DispatchDate: 13.12.2021 · ProofNo: 1254, p.1

nature climate change

ARTICLES

https://doi.org/10.1038/s41558-021-01254-9

A regime shift in seasonal total Antarctic sea ice extent in the twentieth century

Ryan L. Fogt[1]✉, Amanda M. Sleinkofer[1], Marilyn N. Raphael[2] and Mark S. Handcock[3]

In stark contrast to the Arctic, there have been statistically significant positive trends in total Antarctic sea ice extent since 1979. However, the short and highly variable nature of observed Antarctic sea ice extent limits the ability to fully understand the historical context of these recent changes. To meet this challenge, we have created robust, observation-based reconstruction ensembles of seasonal Antarctic sea ice extent since 1905. Using these reconstructions, here we show that the observed period since 1979 is the only time all four seasons demonstrate significant increases in total Antarctic sea ice in the context of the twentieth century and that the observed increases are juxtaposed against statistically significant decreases throughout much of the early and middle twentieth century. These reconstructions provide reliable estimates of seasonally resolved total Antarctic sea ice extent and are skilful enough to better understand aspects of air–sea–ice interactions within the Antarctic climate system.

Sea ice is a critically important component of the very complex Antarctic climate system. Its variability is driven by changes in the atmosphere and ocean, which interact with each other and operate on different timescales[1]. The remote nature of Antarctica means that there are very few in situ measurements of the surrounding atmosphere or ocean where the sea ice forms, and understanding its variability depends largely on satellite observations[2,3]. Satellite measurements of Antarctic sea ice extent indicate weak but statistically significant increases in total sea ice around Antarctica from 1979 to 2016, followed by a sharp decline to below-average values in 2016 and a record low in summer 2017, before returning to average by austral summer 2020. While the total Antarctic sea ice extent exhibits a positive trend[4] (unlike the Arctic sea ice extent[5]), there is a strong regionality[6] and seasonality[7] to the trends, and they can be of opposite signs, particularly marked by an increase in the Ross Sea and a decrease in the Bellingshausen Sea prior to 2016[1,4]. Analyses of the observed temporal and spatial variability in Antarctic sea ice have been attempted[8–12], but a thorough understanding is limited because the sparsity of in situ observations and the brevity of the satellite record mean that their temporal uniqueness cannot be easily assessed[13]. Their future change is also uncertain, since coupled climate models used in both the fifth and the recent sixth IPCC assessment reports fail to reproduce the observed increases; instead, most show widespread decreases around Antarctica[14–16].

To improve understanding of Antarctic sea ice variability, several reconstructions of Antarctic sea ice have been completed[17–20]. While these reconstructions substantially extend the short observational record, they have limitations. Their main challenges are that they represent sea ice conditions only in a certain area (or sometimes at a certain point along the ice edge), and they often can resolve only annual mean sea ice conditions or the sea ice extent during a specific season[17]. Even model-based simulations of past sea ice that assimilate sea ice proxy records are not able to provide more detail on Antarctic sea ice variability, as these are similarly limited by the resolution of the proxy data incorporated into the model[20].

Here we present seasonal reconstructions of Antarctic sea ice extent since 1905 that avoid the shortcomings outlined above, as they are based on physical climate relationships across the southern hemisphere represented by pressure and temperature observations and indices of climate variability patterns. In addition to the total sea ice extent, we use an ensemble approach to separately reconstruct seasonal Antarctic sea ice extent for five sectors that partition the Antarctic region along delineations of temporal variance and spatial decorrelation[21]. This reconstruction ensemble provides estimates of seasonally resolved Antarctic total sea ice extent during the twentieth century.

Antarctic total sea ice extent in the twentieth century

Our ensemble reconstructions (Fig. 1) are based on a principal component (PC) regression model, successfully employed in previous Antarctic climate reconstructions[22–25] (Methods). At the heart of this model is the strong connection that Antarctic sea ice shares with regional and large-scale climate variability, captured through a network of 30 long-term temperature and pressure observations across the southern hemisphere and indices of climate variability extending back to 1905 (Extended Data Fig. 1); different configurations of these predictor data create individual reconstruction ensemble members. To indirectly account for the slower role of the ocean (compared with the atmosphere) in driving Antarctic sea ice changes, we also allow for the predictor data to lead the sea ice by up to one season, at one-month increments (Methods). To assess the reconstruction uncertainty, we verify our reconstructions with an independent leave-one-out cross-validation procedure and use four different skill metrics to evaluate the performance of each ensemble member (Methods and Fig. 2 caption).

The total Antarctic sea ice extent ensemble mean reconstruction (blue lines in Fig. 1), taken as the average of the more than 200,000 sums of sector reconstructions, is well correlated with the observations ($r > 0.79$, $P < 0.01$). Our reconstruction clearly captures the positive trend in observations prior to 2016[4], and the sudden decline in 2016[11,26,27] lies within the reconstruction uncertainty (grey

[1]Department of Geography and Scalia Laboratory for Atmospheric Analysis, Ohio University, Athens, OH, USA. [2]Department of Geography, University of California–Los Angeles, Los Angeles, CA, USA. [3]Department of Statistics, University of California–Los Angeles, Los Angeles, CA, USA. ✉e-mail: fogtr@ohio.edu

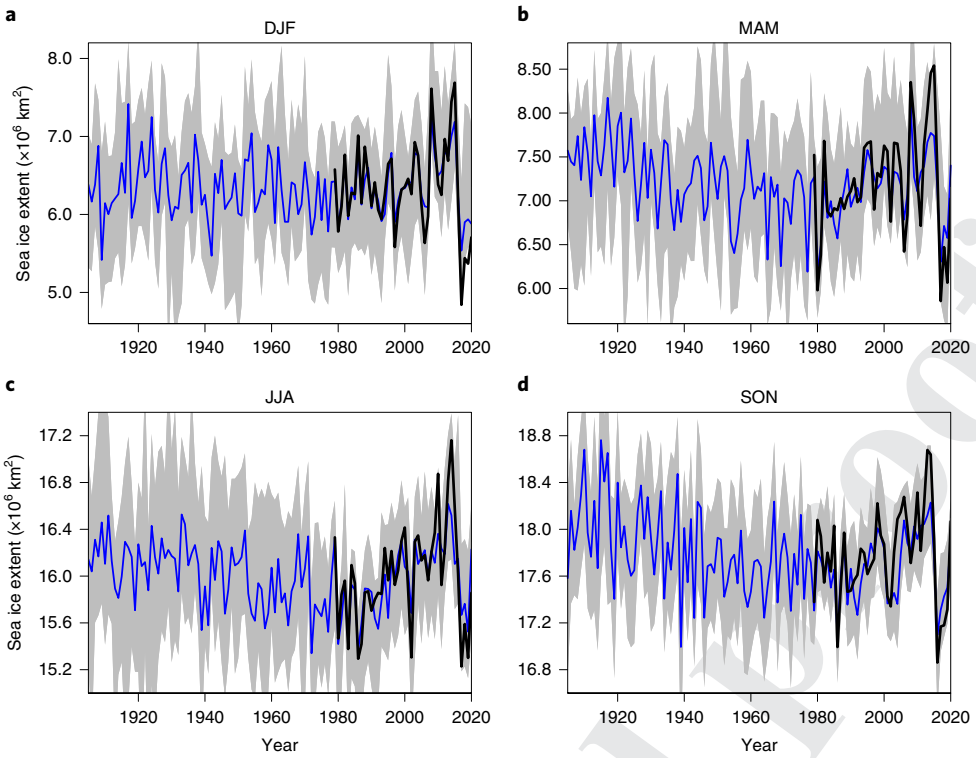

Fig. 1 | Antarctic seasonal total sea ice extent, 1905–2020. a–d, Sea ice observations (black lines) are from the Climate Data Record (CDR) daily concentration fields from the National Oceanic and Atmospheric Administration / National Snow and Ice Data Center (NOAA/NSIDC) CDR of Passive Microwave Sea Ice Concentration, Version 4 (https://nsidc.org/data/g02202)[43]. The blue lines are the ensemble mean reconstructions acquired from the average of over 200,000 possible sums of seasonal sector-based sea ice extent reconstructions, and the grey shading approximates the reconstruction uncertainty as the greater of 1.96 times the standard deviation of the ensemble members or 1.96 times the standard deviation of the residuals of an individual best-fit reconstruction ensemble member. The seasons shown are DJF (**a**), March–May (MAM) (**b**), JJA (**c**) and SON (**d**).

shading in Fig. 1). Since the Antarctic sea ice extent is reconstructed separately for five sectors as well as the total, we can use various sums of the sector reconstructions to further examine the reconstruction performance and provide more detail than previous proxy-based reconstructions[17–20] on the historical variability in total Antarctic sea ice extent (Fig. 2). The correlation of the seasonal total Antarctic sea ice extent represented by three additional reconstructions (see the Fig. 2 caption for the details) with the observed total Antarctic sea ice extent exceeds 0.71 for all seasons for each configuration. Except for September–November (SON), the reconstructions for the sum of the sectors are roughly equally or more highly correlated with the observations than are the reconstructions specifically calibrated to the observed total Antarctic sea ice (red lines). This fact also validates the skill of the sector reconstructions, as their sum was not calibrated to the observed total sea ice extent during the reconstruction model. Furthermore, the correlations (1905–2020) of each reconstruction with the ensemble mean from Fig. 1 (given at the bottom of each panel in Fig. 2) are above 0.49 (comparable to and often exceeding the correlations of existing proxy-based reconstructions with observations)[17–20]. These relatively high correlations among the various reconstruction ensemble members of the total sea ice extent demonstrate that the reconstructions are fairly stationary across the large ensemble and not overly sensitive to particular predictor data. Collectively, the larger variance inherent in the three individual total sea ice reconstructions (compared with the ensemble mean in blue, Fig. 2) allows us to conclude that sudden changes from one year to the next in the total Antarctic sea ice extent as observed from 2016 to 2017 (depending on the season) have occurred numerous times in the past century, including large increases. More broadly, all of the observed Antarctic sea ice extremes since 1979 fall within the historical range of reconstruction uncertainty (Figs. 1 and 2) since 1905.

The overall skill across all possible ensemble members (including reconstructions for each sector as well as the total) further indicates that the reconstructions are robust (Extended Data Fig. 2). The skill metrics for all ensemble reconstructions (blue) are positive (indicating a reconstruction that outperforms the climatological mean), while the reconstructions with the best fit to the observed sea ice extent (red; Methods), a subset of only six reconstructions (one for each sector and the total), have skill metrics at or above ~0.30 (Extended Data Fig. 2). Indeed, the total sea ice extent reconstructions (Figs. 1 and 2) are often less skilful than the regional reconstructions (Extended Data Fig. 2), related to the fact that the total extent is influenced by many regional processes that often offset or cancel each other[1,4,8]. Similar to the reconstructions, sea ice forecasts perform much better for individual sectors than they do for the total Antarctic-wide sea ice[28]. These sectoral differences are also why a circum-Antarctic proxy-based reconstruction has not been possible[17,19].

Comparison with existing proxy-based reconstructions

As expected, there are challenges in comparing our reconstructions with a few proxy-based (here, only using ice cores) reconstructions[18,20,29–31] (Table 1). First, the proxy reconstructions represent only a specific time of year and a certain geographic region, neither of which aligns with our traditional meteorological seasons and distinct Antarctic sea ice sectors. To align more directly, correlations between the proxy reconstructions and observations for comparable seasons and sea ice extent sectors used in this study are presented separately from the published correlations. Except the

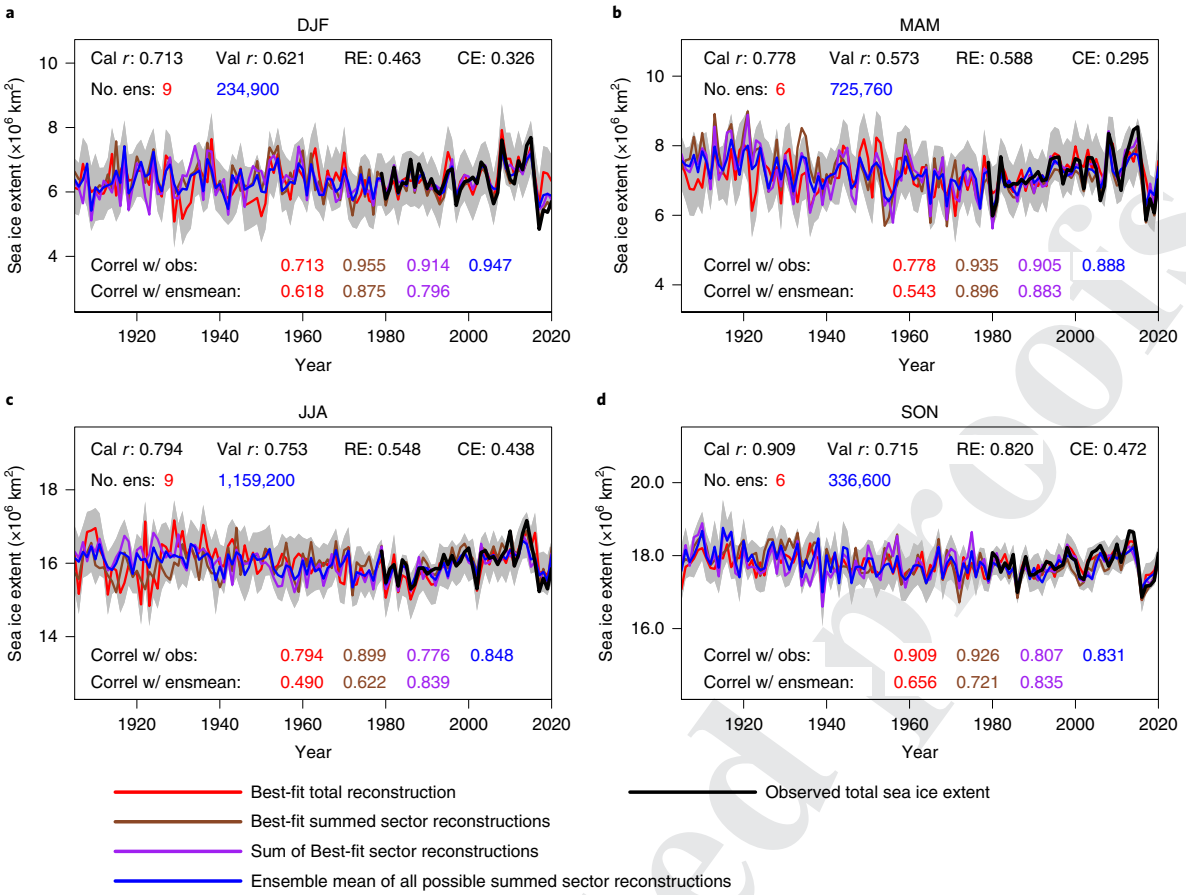

Fig. 2 | Seasonal Antarctic total sea ice extent comparisons, 1905–2020. a–d, Various ways of representing the total Antarctic sea ice extent reconstruction, along with various reconstruction skill metrics for the best-fit reconstruction (red lines). Cal *r*, calibration correlation; val *r*, validation correlation; RE, reduction of error; CE, coefficient of efficiency. The best-fit reconstruction (red lines) is the highest-performing ensemble member calibrated specifically to the observed total sea ice extent. The best-fit summed sector reconstruction (brown lines) is the ensemble member from all possible sums of the individual sector ensemble members, while the ensemble mean (blue lines) is the average of all these possible sector reconstruction sums. The sum of the best-fit sector reconstructions (purple lines) is the sum of the highest-performing sector reconstruction ensemble members that have been specifically calibrated to the observed sector sea ice extent. The correlation of all reconstructions with the observations (correl w/ obs) and the correlation of the reconstructions with the ensemble mean (correl w/ ensmean) are given at the bottom of each plot, with the colours representing the various reconstructions labelled in the legend below the figure. The number of ensemble members (no. ens) is also given for the best-fit reconstruction (red) as well as for the ensemble mean (blue). The grey shading is as in Fig. 1 and approximates the reconstruction uncertainty as the greater of 1.96 times the standard deviation of the ensemble members or 1.96 times the standard deviation of the best-fit reconstruction ensemble member.

reconstruction for sea ice extent near Law Dome in East Antarctica (90° E–110° E)[31], it is clear that the correlations of the proxy-based reconstructions for sectors and seasons comparable to our reconstructions are smaller than their original published correlations. Note, however, that the correlations for the proxy-based reconstructions end much earlier than 2020 (most prior to 2000). Nonetheless, the average correlation of our reconstructions with observations, and nearly all ensemble members (range given in parentheses), exceeds the published correlations of these proxy-based reconstructions over a much larger region, over many different seasons and over a much longer period (1979–2020). The aforementioned differences in the proxy reconstructions make the correlations much weaker after 1979 and near zero for the period of overlap before 1978 (Table 1). Of note, though, is the significant persistent positive correlation of the South Orkney fast ice record[30] with our reconstructions of the Weddell Sea ice extent in both June–August (JJA) and SON throughout the twentieth century. Since this is an observation-based estimate of regional sea ice extent, the stronger similarity between our reconstruction and this estimate continues to suggest that our reconstructions are robust. In contrast, the reduced correlations elsewhere in Table 1 do not necessarily imply lower reconstruction skill: the proxy-based reconstructions are evaluated during a shorter period of overlap with observations, which is then combined with the inherent uncertainty in all of the reconstructions to reduce the overall relationship. Indeed, the correlations between two proxy-based reconstructions for similar regions[20,29] (the last two rows of Table 1) are near zero before 1979; these correlations improve modestly to only ~0.30 when the reconstructions at the exact location (146° W) are compared[20]. Although the interannual correlations of our reconstructions with existing estimates are weak, the majority of these estimates show similar features in the twentieth century. We now analyse the seasonal reconstructions in greater detail.

A regime shift in twentieth-century Antarctic sea ice extent

By nearly tripling the length of the observed data time series, our ensemble reconstructions provide a clear, consistent story of the historical importance of the observed Antarctic sea ice extent trends. Specifically, the reconstructions highlight an important regime shift in Antarctic sea ice that occurred near 1960, just before the satellite

Table 1 | Comparison of select ice-core-based sea ice proxy reconstructions with our observation-based (calibrated) reconstructions

Study details	Published correlation with observations	Comparable region and season	Proxy reconstruction versus comparable region	Correlation (this study) with observations	Correlation (proxy versus calibrated, 1979–end)	Correlation (proxy versus calibrated, 1905–1978)
Abram et al.[18] W. Peninsula 70° W–110° W August–October	0.71 (1973–1995)	ABS, JJA	0.12	0.82 (0.65, 0.92)		−0.03 (−0.22, 0.10)
		ABS, SON	−0.09	0.90 (0.77, 0.97)	−0.03 (−0.15, 0.08)	0.06 (−0.10, 0.23)
		Wedd., JJA	0.41	0.90 (0.83, 0.94)	0.47 (0.39, 0.55)	0.01 (−0.07, 0.12)
		Wedd., SON	0.22	0.92 (0.79, 0.97)	0.22 (0.16, 0.34)	0.04 (−0.05, 0.16)
South Orkney sea ice duration[30] 50° W–10° E August–October	0.79 (1973–1995)	Wedd., JJA	0.53	0.90 (0.83, 0.94)	0.55 (0.46, 0.66)	0.49 (0.32, 0.57)
		Wedd., SON	0.79	0.92 (0.79, 0.97)	0.73 (0.67, 0.78)	0.48 (0.29, 0.57)
Law Dome[31] 90° E–110° E August–October	0.60 (1973–1995)	E. Ant., JJA	0.74	0.82 (0.72, 0.95)	0.47 (0.31, 0.65)	−0.05 (−0.09, 0.04)
		E. Ant., SON	0.63	0.84 (0.67, 0.95)	0.39 (0.19, 0.56)	−0.03 (−0.13, 0.09)
Thomas and Abram[29] 146° W Annual mean	0.64 (1979–2010)	Ross–Amundsen, annual	0.59	0.89 (0.71, 0.96)	0.56 0.38, 0.69)	0.09 (−0.10, 0.36)
		ABS, annual	−0.49	0.88 (0.73, 0.97)	−0.59 (−0.73, −0.42)	−0.04 (−0.36, 0.18)
Dalaiden et al.[20] Ross Sea Annual mean	0.51 (1979–2000)	Ross–Amundsen, annual	0.35	0.89 (0.71, 0.96)	0.38 (0.19, 0.58)	0.09 (−0.13, 0.30)
Dalaiden et al. Bellingshausen Sea Annual mean	0.43 (1979–2000)	ABS, annual	0.59	0.88 (0.73, 0.97)	0.63 (0.46, 0.75)	−0.02 (−0.20, 0.20)
Dalaiden et al. versus Thomas and Abram Ross Sea Annual					0.21	0.03
Dalaiden et al. versus Thomas and Abram Bellingshausen Sea Annual					−0.69	0.03

The details of the proxy-based reconstruction, including the region, seasonality and published correlation with observations (and time period for this correlation), are given in the first two columns. The region from this study most comparable is listed in the third column, and the correlations of the proxy-based reconstructions with the observations from the comparable region are given in the fourth column during the period of overlap. The final columns represent comparisons with our observation-based (calibrated) reconstructions, with the mean correlation and range from all ensemble members (in parentheses) as follows: correlations with observations for the comparable region, correlations between the proxy-based and our observation-based reconstructions from 1979 onwards, and those prior to 1979. ABS, Amundsen–Bellingshausen Seas; Wedd., Weddell Sea; E. Ant., East Antarctica. The final two rows are correlations between two annual mean proxy-based sea ice reconstructions in the South Pacific sector.

observations (Fig. 3). The shift is characterized by a change in the total sea ice extent trend to a new regime that includes the dramatic persistent decline of sea ice that began in 2016.

In terms of the changes in Antarctic sea ice trends, the shorter observational period (Fig. 3a,f,k,p) shows strong positive trends especially for periods ending in 2014 (its record maximum based on satellite measurements[4]) to 2016, prior to the marked decline. The increase in total Antarctic sea ice extent over the satellite record contrasts with the rapid, widespread declines in Arctic sea ice over the same period[5]. However, these trends are based on only a little over 40 years of observed satellite data (visualized as the small box in the upper-right panels of the remaining four columns of Fig. 3), making it a challenge to resolve decadal-scale variability and assess the trends' historical significance from observations alone[13]. In comparison, trends from the reconstructions for various periods throughout the twentieth century highlight that the positive trends since 1979 (in both observations and reconstructions) are unique in the context of Antarctic sea ice variability over the twentieth century. Our reconstructions, which fully resolve variations across the seasons, show here that these are the only statistically significant ($P<0.10$) increases in Antarctic sea ice extent for any period simultaneously in all four seasons since 1905 (Fig. 3).

Moreover, in most seasons, the positive trends in the observational period stand in marked contrast to statistically significant ($P<0.10$) negative trends in the early to mid-twentieth century, especially prevalent in the ensemble mean (Figs. 1 and 3e,j,o,t). The negative trends in the early to mid-twentieth century reach statistical significance ($P<0.05$, stippled in Fig. 3) in all but December–February (DJF). Combined with the short observational time series, the reconstructions strongly suggest a regime shift in Antarctic sea ice extent in the middle of the twentieth century, where long-term declines in Antarctic sea ice extent before 1960 are juxtaposed by strong increases in the late twentieth century, which encompass the satellite observations (Fig. 3, left column and boxes in the other columns). These trends also suggest that the observed period started at a time of relatively low sea ice extent in the context of the last century, giving rise to a positive trend that is part of multidecadal variability (Figs. 1 and 2).

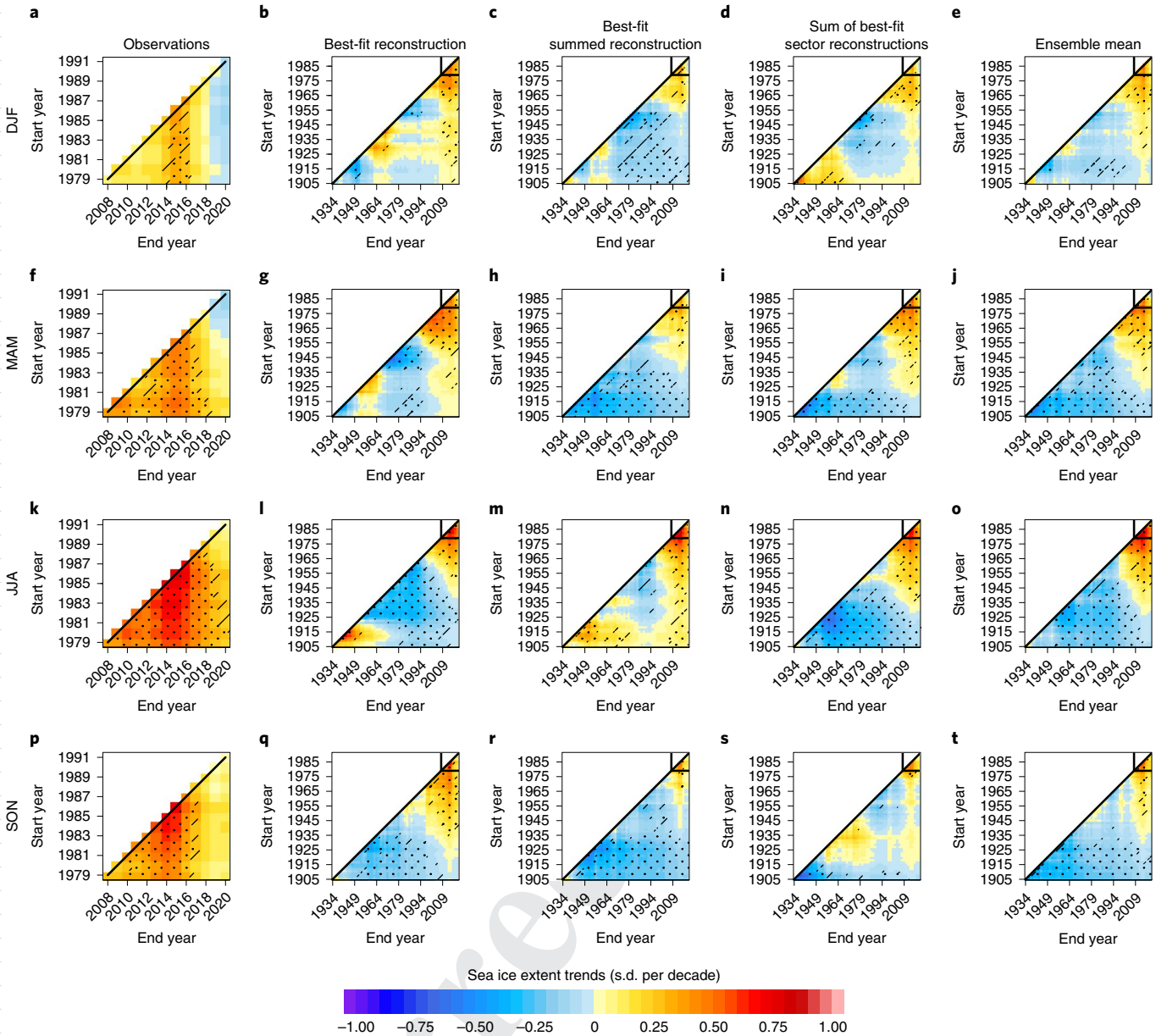

Fig. 3 | Time-varying linear trends of standardized seasonal Antarctic total sea ice extent. a–t, The *y* axis identifies the starting year for a trend, and the *x* axis the ending year for a trend, so that shorter periods are in the upper left and longer periods in the lower right of each panel. The diagonal line is exactly 30 years, and trends are given only for periods 30 years or longer. The observations are in the far left column (**a**,**f**,**k**,**p**, with different start and end periods than the other columns), and the remaining columns (labelled at the top of the plot) represent estimates of the total Antarctic sea ice as described in Fig. 2; the boxes drawn in the upper right corners of the reconstruction trends represent the short period of Antarctic sea ice extent observations from satellites. The cross-hatching and stippling represent trends that are significantly different from zero at $P < 0.10$ and $P < 0.05$, respectively.

Importantly, many other proxy-based reconstructions of Antarctic sea ice extent hint at a similar (but weaker) reversal of sea ice changes from the early to late twentieth century, especially in the Ross and Weddell Seas[17,18,20]. Although the observed trends are not produced as well as our reconstructions, recent Antarctic sea ice extent reconstructions[19] based on six proxies similarly confirm a mid-twentieth-century regime shift in Antarctic sea ice, with widespread decreases in annual mean extent in many sectors in the early to mid-twentieth century that switch to increases during the observed satellite period. As such, even with weak interannual correlations between our reconstructions and various proxy-based reconstructions (Table 1), the majority of published estimates suggest a similar reversal in Antarctic sea ice trends in the mid-twentieth century.

Our reconstruction approach allows further examination of the regime shift in total Antarctic sea ice extent in austral winter (JJA, Fig. 3o) for each sector separately (Fig. 4). It is clear that the regime shift is not equally pronounced in all sectors, highlighting the known independent nature of Antarctic sea ice in various sectors around the continent[21]. Indeed, the regime shift from early to mid-twentieth-century ice loss to late twentieth-century ice gains is the most pronounced in the King Hakon VII and Ross–Amundsen Seas sectors (Fig. 4b,d). For the Ross–Amundsen Seas, our best-fit reconstruction indicates that the JJA sea ice decreased by 0.206 ± 0.099 standard deviations per decade ($P < 0.01$) during 1905–1978, followed by an increase of 0.307 ± 0.224 standard deviations per decade ($P < 0.05$) from 1979 to 2020; the

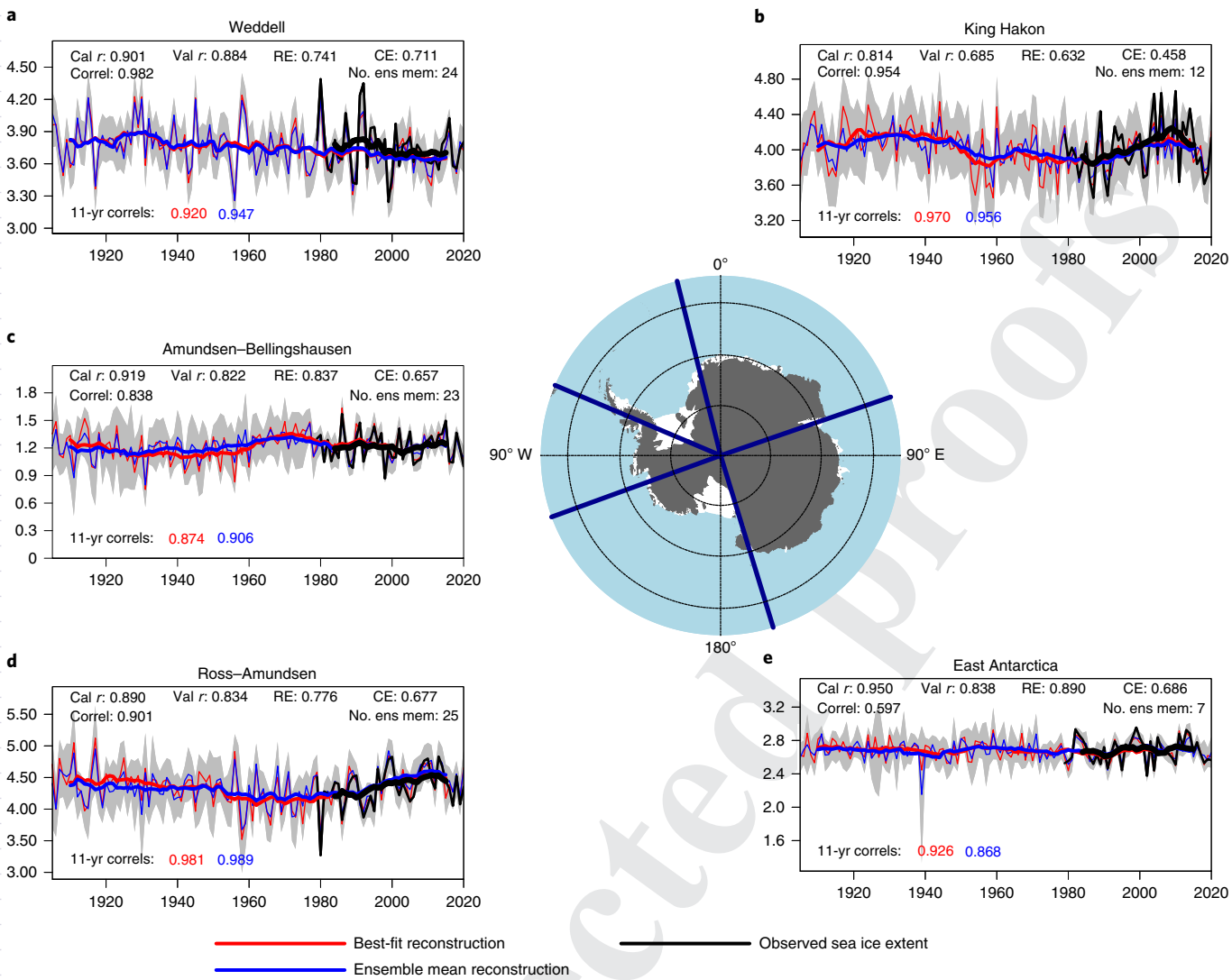

Fig. 4 | Austral winter (JJA) sea ice extent reconstructions by sector. a, Weddell Sea (250° E–346° E). **b**, King Hakon VII (346° E–71° E). **c**, Amundsen–Bellingshausen Seas (250° E–290° E). **d**, Ross–Amundsen Seas (162° E–250° E). **e**, East Antarctica (71° E–162° E). The thick lines are smoothed versions (with an 11-year running mean) of each time series. Given in each panel are the reconstruction skill metrics (detailed in Fig. 1) for the best-fit reconstruction (red line), as well as the correlation between the ensemble mean and the best-fit reconstruction during 1905–2020 (correl). The number of ensemble reconstructions produced is given in the upper right, and the correlations of the 11-year smoothed versions with the observed smoothed data are given at the bottom, with the colours representing the best-fit (red) or ensemble mean (blue) reconstructions. The grey shading in each panel represents the reconstruction uncertainty, taken as the larger of 1.96 times the standard deviation of the best-fit reconstruction compared to the observed, or 1.96 times the standard deviation of the reconstruction ensembles for a given year.

Ross–Amundsen Seas is the only sector to display a statistically significant ($P<0.05$) increase in winter Antarctic sea ice extent during 1979–2020 in our reconstructions and observations (the observed trend is $+0.268\pm0.239$ standard deviations per decade). Similarly supporting a regime shift, the 1905–1978 trend (-0.160 ± 0.109 standard deviations per decade, $P<0.01$) and the 1979–2020 trend ($+0.177+0.206$ standard deviations per decade, $P<0.10$) in the best-fit reconstruction for the King Hakon sector are statistically different from each other ($P<0.05$).

Consistent with sea ice trends during the satellite era[10,12,32], our sector reconstructions also clearly indicate an offsetting behaviour between the Ross–Amundsen (Fig. 4d) and Amundsen–Bellingshausen Seas (Fig. 4c) throughout the twentieth century. In the Amundsen–Bellingshausen Seas, the winter ensemble mean reconstruction demonstrates that sea ice was increasing during 1905–1978 (0.140 ± 0.103 standard deviations per decade, $P<0.01$), in opposition to the decreases in the Ross–Amundsen sector during the same period (Fig. 4d). The winter trend switched to a weak and statistically insignificant negative trend after 1979 in the Amundsen–Bellingshausen Seas, similar to the observations, and again in opposition to the change in the Ross–Amundsen Seas (Fig. 4c,d). We note, however, that when analysed separately, there is a statistically significant negative trend in the observations for the Bellingshausen Sea[1,4,8]. The opposing behaviour between the Ross and Bellingshausen Seas, at least in observations, can largely be linked to changes in the atmospheric circulation related to the Amundsen Sea Low, a semipermanent region of low pressure. When particularly strong, the winds associated with the Amundsen Sea Low act to push sea ice towards the Antarctic coast and peninsula in the Bellingshausen Sea, while pushing it equatorwards in the nearby Ross Sea[6,10,33,34]. Our finding supporting the persistence in the twentieth century of the observed opposing relationship between the

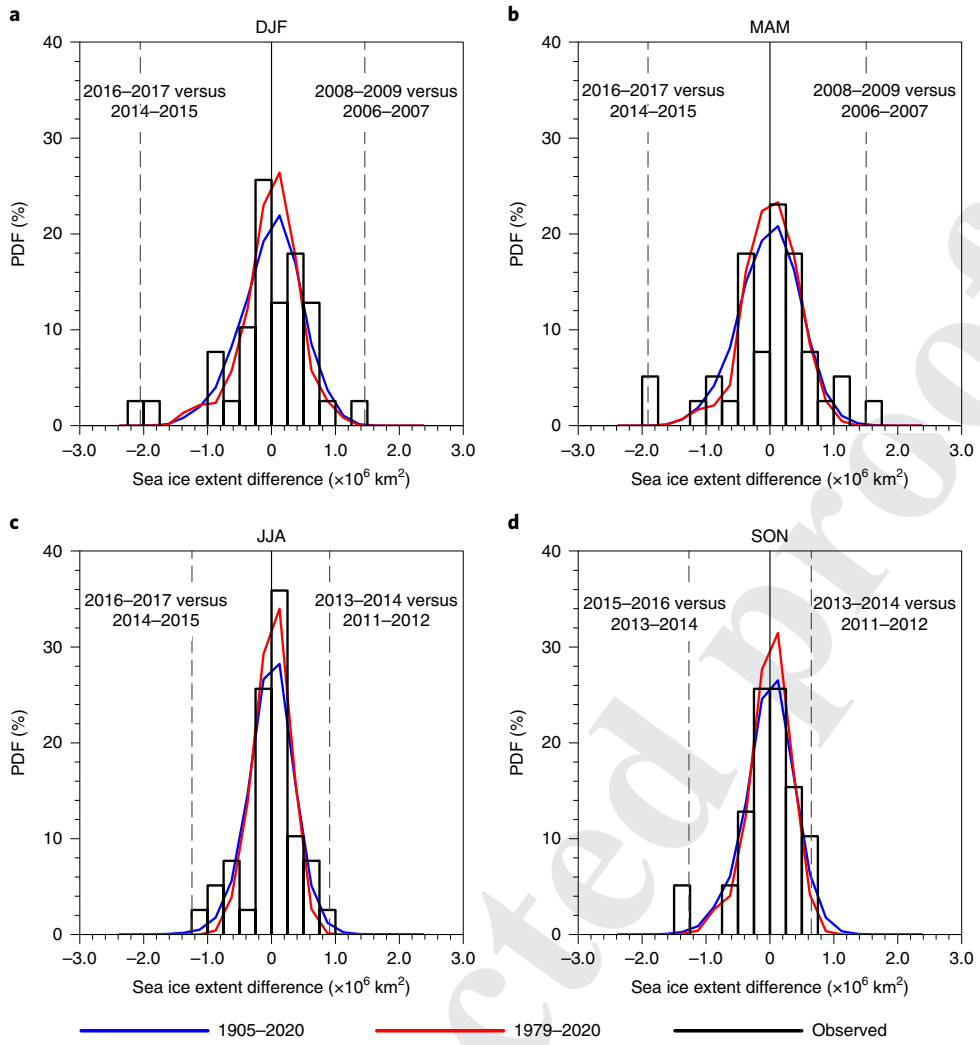

Fig. 5 | Changes in two-year average seasonal sea ice extent. a–d, Seasonal probability distribution functions (PDFs, in %) for differences (following years minus preceding years) in consecutive, non-overlapping two-year mean Antarctic total sea ice extent from observations (black, plotted as a bar chart) and in all Antarctic total sea ice extent reconstruction ensemble members from 1979 to 2020 (red) and 1905 to 2020 (blue). The dashed vertical lines indicate the minimum and maximum differences in the observations, with the two-year mean periods corresponding to these record differences given in the upper corners of each panel.

Ross and Amundsen–Bellingshausen Seas was also found in another Antarctic sea ice extent reconstruction study[20], although that study did demonstrate persistent declines in the Bellingshausen Sea in the twentieth century, similar to other reconstruction studies[18,29]. While these differences in trends might suggest lower reconstruction confidence for our reconstructions in the Amundsen–Bellingshausen Seas, these proxy-based reconstructions more closely align to observations from the Weddell or Ross–Amundsen Seas than to observations in the Amundsen–Bellingshausen Seas (Table 1). Our reconstructions similarly produce negative trends before 1978 in both the Ross–Amundsen and Weddell Seas in winter, suggesting similarity in our work and existing estimates after adjusting for the spatial disparities among the various reconstructions. Regardless, we urge caution in only using specific periods to investigate trends within a longer time series, as the trends (in both magnitude and statistical significance) are sensitive to the starting and ending dates, and the regime shift does not begin simultaneously across the sectors (Fig. 4) or across the various ensemble members in the reconstruction (Fig. 3).

Although the Antarctic sea ice regime shift is strongly pronounced in the changing trends through time, the new regime since ~1960 can also be characterized by persistent years of below-average sea ice extent, which began in 2016. As mentioned earlier, our reconstructions capture the magnitude of the observed changes from one year to the next in total sea ice extent (Fig. 2), further depicted in the probability distribution functions of year-to-year sea ice changes in observations and our reconstruction ensemble (Extended Data Fig. 3). However, given that the total Antarctic sea ice extent had been consistently increasing before 2016 (Fig. 3) and then remained below average for several years after 2016 (Fig. 1), changes in the average sea ice between two consecutive, non-overlapping years emerge as unique characteristics of the recent Antarctic total sea ice extent regime that includes the 2016 event (Fig. 5). The extreme change in relatively high (equatorward) sea ice extent for the two years immediately before 2016 and the persistent decline for the following two years fall outside the range of extreme changes in our reconstructions, including those only during the 1979–2020 period. However, the differences between the reconstructions and observations in Fig. 5 are not statistically significant (Methods), except for DJF ($P=0.01$). Thus, while our large reconstruction ensemble indicates that pronounced changes from one year to the next are common features in seasonal total Antarctic sea ice variability

(Extended Data Fig. 3), the switch from persistently above-average to persistently below-average Antarctic total sea ice extent that characterized the 2016 event has occurred infrequently since the beginning of the twentieth century.

Discussion

Given the complexities of the Antarctic sea ice trends (both spatially and temporally), interpreting the causality of the pronounced regime shift remains a challenge. Meteorological records near Antarctica generally only reach back to the International Geophysical Year (1957–1958)[35]. Because the sea ice trends changed sign around 1960, there is not a pronounced signal in many of the closest meteorological measurements[36,37], although at least one study does indicate a reversal in pressure, temperature and zonal wind trends across the Southern Ocean (including coastal Antarctica) near 1979[38]. Attribution studies are further complicated since climate models generally produce widespread Antarctic sea ice loss since 1979, contrary to observations[14–16]. Yet, some sea ice proxy-based reconstructions suggest reversals in the twentieth century[19,20], including one that highlights the unique nature of the most recent 30-year period[29], similar to our results.

Nonetheless, the regional and time-sensitive character of the reversal strongly hints at the important role of pronounced decadal-scale variability in both the atmosphere and the ocean. Observations of the ocean near Antarctica are even sparser, but previous work suggests that convection in the Southern Ocean contributes strongly to observed trends in temperature and sea ice near Antarctica, especially on longer timescales[1,38,39]. From the atmospheric perspective, many of the midlatitude pressure observations used as predictors here show patterns of decadally varying trends with synchronous but opposing variability between the mid- and high latitudes of the southern hemisphere[40], primarily associated with the Southern Annular Mode (SAM). Other work has suggested the influence of the SAM on mid-twentieth-century Antarctic sea ice regime shifts[19]; however, the SAM index used in that study (based on gridded atmospheric reanalysis products spanning the entire twentieth century) is known to have artificial trends throughout the twentieth century[41,42]. Perhaps tied to the regional variations in the trends, shifts in the Interdecadal Pacific Oscillation (IPO, negative trends in the early and late twentieth century to positive trends in the mid-twentieth century), a pattern known to impact Antarctic sea ice variations from the Ross to Weddell Seas[11,12,32], probably also play an important role[40]. Given that all the JJA best-fit reconstructions from the Ross–Amundsen eastwards to the Weddell Sea in Fig. 4 employ many different subsets of tropical sea surface temperature (SST) indices, including the IPO, the importance of decadal-scale tropical variability cannot be overstated.

Analysis of these contributions is part of future work, but hopefully the reconstructions presented here will promote an increase in research from many disciplines aimed at further interpreting and unlocking historical variations in Antarctic sea ice extent during the twentieth century. As these reconstructions are highly skilful, they are also appropriate to use in further research on evaluating climate models and interpreting the causes of the regime shifts depicted in these reconstructions. Further work could also employ these reconstructions along with other reconstructions and observations (pressure, temperature, SAM and so on) to better understand the interconnected southern hemisphere climate system.

Online content

Any methods, additional references, Nature Research reporting summaries, source data, extended data, supplementary information, acknowledgements, peer review information; details of author contributions and competing interests; and statements of data and code availability are available at https://doi.org/10.1038/s41558-021-01254-9.

Received: 19 August 2021; Accepted: 24 November 2021;

References

1. Hobbs, W. R. et al. A review of recent changes in Southern Ocean sea ice, their drivers and forcings. *Glob. Planet. Change* **143**, 228–250 (2016).
2. Cavalieri, D. J. & Parkinson, C. L. Antarctic sea ice variability and trends, 1979–2006. *J. Geophys. Res.* https://doi.org/10.1029/2007JC004564 (2008).
3. Parkinson, C. L. & Cavalieri, D. J. Antarctic sea ice variability and trends, 1979–2010. *Cryosphere* **6**, 871–880 (2012).
4. Parkinson, C. L. A 40-y record reveals gradual Antarctic sea ice increases followed by decreases at rates far exceeding the rates seen in the Arctic. *Proc. Natl Acad. Sci. USA* **116**, 14414–14423 (2019).
5. Stroeve, J. & Notz, D. Changing state of Arctic sea ice across all seasons. *Environ. Res. Lett.* **13**, 103001 (2018).
6. Turner, J., Hosking, J. S., Bracegirdle, T. J., Marshall, G. J. & Phillips, T. Recent changes in Antarctic sea ice. *Phil. Trans. R. Soc. Math. Phys. Eng. Sci.* **373**, 20140163 (2015).
7. Holland, P. R. The seasonality of Antarctic sea ice trends. *Geophys. Res. Lett.* **41**, 4230–4237 (2014).
8. Stammerjohn, S. et al. The influence of winds, sea-surface temperature and precipitation anomalies on Antarctic regional sea-ice conditions during IPY 2007. *Deep Sea Res. 2 Top. Stud. Oceanogr.* **58**, 999–1018 (2011).
9. Stammerjohn, S. E., Martinson, D. G., Smith, R. C., Yuan, X. & Rind, D. Trends in Antarctic annual sea ice retreat and advance and their relation to El Niño–Southern Oscillation and Southern Annular Mode variability. *J. Geophys. Res.* https://doi.org/10.1029/2007JC004269 (2008).
10. Holland, P. R. & Kwok, R. Wind-driven trends in Antarctic sea-ice drift. *Nat. Geosci.* **5**, 872–875 (2012).
11. Purich, A. & England, M. H. Tropical teleconnections to Antarctic sea ice during austral spring 2016 in coupled pacemaker experiments. *Geophys. Res. Lett.* https://doi.org/10.1029/2019GL082671 (2019).
12. Meehl, G. A., Arblaster, J. M., Bitz, C. M., Chung, C. T. Y. & Teng, H. Antarctic sea-ice expansion between 2000 and 2014 driven by tropical Pacific decadal climate variability. *Nat. Geosci.* **9**, 590–595 (2016).
13. Jones, J. M. et al. Assessing recent trends in high-latitude southern hemisphere surface climate. *Nat. Clim. Change* **6**, 917–926 (2016).
14. Turner, J., Bracegirdle, T. J., Phillips, T., Marshall, G. J. & Hosking, J. S. An initial assessment of Antarctic sea ice extent in the CMIP5 models. *J. Clim.* **26**, 1473–1484 (2013).
15. Shu, Q. et al. Assessment of sea ice extent in CMIP6 with comparison to observations and CMIP5. *Geophys. Res. Lett.* https://doi.org/10.1029/2020GL087965 (2020).
16. Roach, L. A. et al. Antarctic sea ice area in CMIP6. *Geophys. Res. Lett.* https://doi.org/10.1029/2019GL086729 (2020).
17. Thomas, E. R. et al. Antarctic sea ice proxies from marine and ice core archives suitable for reconstructing sea ice over the past 2000 years. *Geosciences* **9**, 506 (2019).
18. Abram, N. J. et al. Ice core evidence for a 20th century decline of sea ice in the Bellingshausen Sea, Antarctica. *J. Geophys. Res.* https://doi.org/10.1029/2010JD014644 (2010).
19. Yang, J., Xiao, C., Liu, J., Li, S. & Qin, D. Variability of Antarctic sea ice extent over the past 200 years. *Sci. Bull.* https://doi.org/10.1016/j.scib.2021.07.028 (2021).
20. Dalaiden, Q., Goosse, H., Rezsohazy, J. & Thomas, E. R. Reconstructing atmospheric circulation and sea-ice extent in the West Antarctic over the past 200 years using data assimilation. Preprint at *Research Square* https://doi.org/10.21203/rs.3.rs-224001/v1 (2021).
21. Raphael, M. N. & Hobbs, W. The influence of the large-scale atmospheric circulation on Antarctic sea ice during ice advance and retreat seasons. *Geophys. Res. Lett.* **41**, 5037–5045 (2014).
22. Fogt, R. L. et al. Antarctic station-based seasonal pressure reconstructions since 1905. 1. Reconstruction evaluation: Antarctic pressure evaluation. *J. Geophys. Res. Atmos.* **121**, 2814–2835 (2016).
23. Fogt, R. L. et al. A twentieth century perspective on summer Antarctic pressure change and variability and contributions from tropical SSTs and ozone depletion. *Geophys. Res. Lett.* **44**, 9918–9927 (2017).
24. Jones, J. M. et al. Historical SAM variability. Part I: century-length seasonal reconstructions. *J. Clim.* **22**, 5319–5345 (2009).
25. Fogt, R. L. et al. Seasonal Antarctic pressure variability during the twentieth century from spatially complete reconstructions and CAM5 simulations. *Clim. Dyn.* https://doi.org/10.1007/s00382-019-04674-8 (2019).
26. Turner, J. et al. Recent decrease of summer sea ice in the Weddell Sea, Antarctica. *Geophys. Res. Lett.* https://doi.org/10.1029/2020GL087127 (2020).
27. Stuecker, M. F., Bitz, C. M. & Armour, K. C. Conditions leading to the unprecedented low Antarctic sea ice extent during the 2016 austral spring season. *Geophys. Res. Lett.* **44**, 9008–9019 (2017).

28. Bushuk, M. et al. Seasonal prediction and predictability of regional Antarctic sea ice. *J. Clim.* https://doi.org/10.1175/JCLI-D-20-0965.1 (2021).
29. Thomas, E. R. & Abram, N. J. Ice core reconstruction of sea ice change in the Amundsen–Ross Seas since 1702 A.D. *Geophys. Res. Lett.* **43**, 5309–5317 (2016).
30. Murphy, E. J., Clarke, A., Symon, C. & Priddle, J. Temporal variation in Antarctic sea-ice: analysis of a long term fast-ice record from the South Orkney Islands. *Deep Sea Res. 1 Oceanogr. Res. Pap.* **42**, 1045–1062 (1995).
31. Curran, M. A. J., van Ommen, T. D., Morgan, V. I., Phillips, K. L. & Palmer, A. S. Ice core evidence for Antarctic sea ice decline since the 1950s. *Science* **302**, 1203–1206 (2003).
32. Purich, A. et al. Tropical Pacific SST drivers of recent Antarctic sea ice trends. *J. Clim.* **29**, 8931–8948 (2016).
33. Raphael, M. N. et al. The Amundsen Sea Low: variability, change, and impact on Antarctic climate. *Bull. Am. Meteorol. Soc.* **97**, 111–121 (2016).
34. Hosking, J. S., Orr, A., Marshall, G. J., Turner, J. & Phillips, T. The influence of the Amundsen–Bellingshausen Seas low on the climate of west Antarctica and its representation in coupled climate model simulations. *J. Clim.* **26**, 6633–6648 (2013).
35. Turner, J. et al. The SCAR READER project: toward a high-quality database of mean Antarctic meteorological observations. *J. Clim.* **17**, 2890–2898 (2004).
36. Turner, J. et al. Antarctic climate change during the last 50 years. *Int. J. Climatol.* **25**, 279–294 (2005).
37. Turner, J. et al. Antarctic temperature variability and change from station data. *Int. J. Climatol.* https://doi.org/10.1002/joc.6378 (2019).
38. Fan, T., Deser, C. & Schneider, D. P. Recent Antarctic sea ice trends in the context of Southern Ocean surface climate variations since 1950. *Geophys. Res. Lett.* **41**, 2419–2426 (2014).
39. Zhang, L., Delworth, T. L., Cooke, W. & Yang, X. Natural variability of southern ocean convection as a driver of observed climate trends. *Nat. Clim. Change* **9**, 59–65 (2019).
40. Fogt, R. L. & Connolly, C. J. Extratropical southern hemisphere synchronous pressure variability in the early twentieth century. *J. Clim.* **34**, 5795–5811 (2021).
41. Fogt, R. L. et al. Historical SAM variability. Part II: twentieth-century variability and trends from reconstructions, observations, and the IPCC AR4 models. *J. Clim.* **22**, 5346–5365 (2009).
42. Schneider, D. P. & Fogt, R. L. Artifacts in century-length atmospheric and coupled reanalyses over Antarctica due to historical data availability. *Geophys. Res. Lett.* **45**, 964–973 (2018).
43. Meier, W., Fetterer, F., Windnagel, A. & Stewart, S. *NOAA/NSIDC Climate Data Record of Passive Microwave Sea Ice Concentration* Version 4 (NOAA/NSIDC, 2021); https://doi.org/10.7265/EFMZ-2T65

Methods

Data and data availability. The seasonal sea ice extent reconstructions are primarily based on monthly mean pressure and temperature records across the southern hemisphere extratropics and midlatitudes from 1905 to 2020. These records were used in previous research[22,40] and obtained from the University Corporation for Atmospheric Research data archive dataset ds570.0 (https://rda.ucar.edu/datasets/ds570.0/#!description)[44]. A few stations were patched with nearby stations using a monthly mean offset, as discussed in earlier work[40]. Of particular note is the station Orcadas, situated near the Antarctic Peninsula, which is the longest continuous atmospheric record polewards of 60° S[45]. Data for the stations in South Africa (Cape Town, Durban and Port Elizabeth) were updated through 2020 by creating monthly means from the daily data in the National Centers for Environmental Information Global Surface Summary of the Day dataset (https://www.ncei.noaa.gov/access/metadata/landing-page/bin/iso?id=gov.noaa.ncdc:C00516)[46]. We have also employed the corrected temperature and pressure measurements for St. Helena Island, which remove the gaps and differences due to station moves through time[47].

Beyond the direct observations of temperature and pressure, indices of modes of climate variability were also used as potential predictors of Antarctic sea ice extent. These include the IPO[48], which is calculated using the difference in SST anomalies averaged in the central equatorial Pacific, the northwest Pacific and the southwest Pacific from the NOAA Extended Reconstructed Sea Surface Temperature dataset, version 5 (ERSSTv5)[49], and the Pacific Decadal Oscillation[50], which is similar to the IPO but includes only tropical and northern Pacific SST anomalies. We also calculated the Niño SST indices from ERSSTv5—namely, the Niño 1+2 SSTs (averaged over 0°–10° S, 270° E–280° E), the Niño 3 SSTs (5° N–5° S, 210° E–270° E), the Niño 3.4 SSTs (5° N–5° S, 190° E–240° E) and the Niño 4 SSTs (5° N–5° S, 160° E–210° E). In addition to these SSTs, to monitor the variability associated with these SSTs and thus monitor the El Niño–Southern Oscillation, we also used the Southern Oscillation Index, the difference in standardized pressure from Tahiti, French Polynesia, and Darwin, Australia, from the Australian Bureau of Meteorology, as it does not have any gaps in the twentieth century (http://www.bom.gov.au/climate/current/soihtm1.shtml). We also used the index for the Atlantic Multidecadal Oscillation[51]. For the SAM index[52], we merged the 'Fogt' seasonal SAM index reconstructions[24,41], which extend back to at least 1905 (http://polarmet.osu.edu/ACD/sam/sam_recon.html), with the observation-based SAM index[53] after 1957 (http://www.nerc-bas.ac.uk/icd/gjma/sam.html). In contrast to the other indices, the SAM indices are only available seasonally; all other predictor data are available for each month. Seven of the nine climate indices are based on ocean variability, and their inclusion as potential predictors therefore helps depict important patterns of climate known to influence Antarctic sea ice that are not fully captured in our geographically limited (to land surfaces) temperature and pressure data.

We computed sea ice extent using satellite-observed sea ice data from the Nimbus-7 Scanning Multichannel Microwave Radiometer and the Defense Meteorological Satellite Program Special Sensor Microwave Imager—Special Sensor Microwave Imager/Sounder (SSM/I-SSMIS). We used the CDR daily concentration fields from the NOAA/NSIDC CDR of Passive Microwave Sea Ice Concentration, Version 4 (https://nsidc.org/data/g02202)[43]. The CDR algorithm output combines ice concentration estimates from the National Aeronautics and Space Administration (NASA) Team algorithm[54] and the NASA Bootstrap algorithm[55]. The data span the period 25 October 1978 to 31 December 2020 and are daily except before July 1987, when they are given every other day. The data are gridded on the SSM/I-SSMIS polar stereographic grid (25 km × 25 km). The sea ice extent used in our analysis is calculated using the equatorward limit of the 15% sea ice concentration isoline. It is thus the sum of the area of every grid cell that is 15% or more covered with sea ice. The monthly sea ice extent was calculated as the average of the sea ice extent for days in that month. In addition to the alternate-day observations from 1978 to 1987, there are a number of days and segments of days with no observations. In particular, there are no data between 3 December 1987 and 12 January 1988. For these days, we fit a stochastically imputed daily sea ice extent using the following procedure. We constructed anomalies by subtracting the invariant annual cycle, estimated using the methods of recent work[56]. We then fit a Bayesian AutoRegressive Integrated Moving Average model to the observed daily sea ice extent. We then stochastically imputed the missing days by drawing from their posterior distribution. The monthly sea ice extent values were computed by averaging all days in the month. We note that, except for the period from 3 December 1987to 12 January 1988, the impact of this stochastic multiple imputation scheme is small, since the daily data are nearly complete. The sectoral sea ice extent was computed as the sum of the area within the sector of every grid cell that is above 15% or more covered with sea ice (most cells are completely within a single sector and do not cross into the adjacent sector). Although contiguous, the sectors are defined on the basis of their spatial decorrelation scale, as discussed in earlier work[21]. The longitude bounds for the sectors are as follows: Amundsen–Bellingshausen Seas (250° E–290° E), Weddell Sea (250° E–346° E), King Hakon VII (346° E–71° E), East Antarctica (71° E–162° E) and Ross–Amundsen Seas (162° E–250° E). The total Antarctic sea ice extent represents the area of all sea ice surrounding Antarctica and is precisely equal to the sum of the areas in the five sectors.

Reconstruction methodology. The seasonal sea ice extent reconstructions follow previous work on early Antarctic climate using a proven PC regression technique[22,23,25,57]. We first compute seasonal means of the various predictor data and correlate these with the sea ice extent time series that is being reconstructed; all data are linearly detrended prior to correlation. To indirectly account for the slower response of the sea ice to the atmosphere and the role of the ocean in this relationship (which also responds slower than the atmosphere), we also correlate predictor data, which lead the Antarctic sea ice extent data for up to one season, at increments of one month. For example, if reconstructing sea ice extent for JJA, the correlations of predictors with JJA sea ice extent are computed for predictor data averaged in JJA (no lag), May–July (MJJ, one-month lead), April–June (AMJ, two-month lead) and MAM (three-month or one-season lead). We note that our reconstructions are skilful only when this lag effect is included as part of our reconstruction procedure.

We perform one separate ensemble reconstruction using all temperature and pressure observations (regardless of correlation magnitude) and smaller networks of predictor data, including indices of climate variability (Extended Data Fig. 1), that are significantly correlated (of detrended data) at $P<0.10$, $P<0.05$, $P<0.025$ and $P<0.01$. For a given correlation threshold (for example, $P<0.10$), we first create an additional ensemble reconstruction based on all the retained temperature and pressure observations significant at the given threshold. We then create additional ensemble reconstructions, as necessary, one at a time by adding to the retained observations any climate indices that are significantly correlated at the given threshold. These increasing smaller sets of predictor data comprise our predictor data networks (four total). The various iterations of any significantly correlated observations and climate indices constitute our data layers. The climate index layers (in order of layering) are the IPO, the Atlantic Multidecadal Oscillation, the Pacific Decadal Oscillation, the Southern Oscillation Index, the Niño 1+2 SSTs, the Niño 3.4 SSTs, the Niño 3 SSTs, the Niño 4 SSTs and the SAM index. Altogether, the combination of data predictor networks (based on the significance of the correlation between predictors and the sea ice extent time series we are reconstructing) and the data layers (adding on to the observations-only layer any significantly correlated climate indices) constitutes a possibility of up to 41 ensemble members for each reconstruction (four data networks times ten data layers plus one ensemble member that employs all observations regardless of correlation magnitude).

Once the predictor data are selected using the above procedure, PC analysis is performed using the retained standardized predictor data (each variable is standardized over the period 1905–2020), including predictor data that lead the sea ice by up to one season. We limit the number of factors calculated in the PC analysis to a maximum of 35 to expedite the computations. A subset of these PCs, sorted by the absolute magnitude of their correlation with the sea ice extent time series being reconstructed, is then regressed onto the sea ice extent time series during 1979–2020 (our calibration period) to fit the reconstruction model. The reconstruction can then be obtained using the relationships that the PCs share with the sea ice extent time series (the regression coefficients) and the relationships that the PCs share with the individual predictor data (the PC expansion weights). Combining the regression and PC weights through matrix multiplications yields a value for each predictor variable, sometimes called the beta weights. These beta weights can then be used on the full length of the observed predictor data to obtain the reconstruction back to 1905. Alternatively, the PCs can similarly be extended back to 1905 from the predictor data and these PCs used with the regression coefficients to perform the reconstruction.

The ideal number of PCs to retain for the regression model is based on an independent validation procedure (leave-one-out cross validation) employed in previous work[22,23,25]. Here we repeat the PC regression model one time for each year in the observed record (calibration period) from 1979 to 2020 (42 times), each time leaving out an individual year and its two neighbouring years before and after (a total of up to five years). The centre year is thus assumed to be independent of the remaining retained years and is predicted using the weights generated in the reconstruction model described above. Predicting each year independently and concatenating the predicted values yields an entirely predicted and independent time series that we call the validation reconstruction. This reconstruction is correlated to the observed sea ice extent data (giving the skill metric that we call validation correlation, or val r) and used separately to compute the CE, as discussed in earlier work[58]. After the CE is determined, the entire validation procedure is repeated by adding one more PC at a time to the regression model. The reconstruction that yields the highest CE is retained as the best-performing ensemble reconstruction for that particular data network and data layer. Selecting the highest CE aids in limiting model overfitting, as the CE will reach a peak, sharply decline and often go very negative as more PCs are added to the regression; this sudden decline is a key indicator of model overfitting despite the overall calibration correlation continuing to increase. Furthermore, retaining only a subset of the PCs makes this regression approach superior to multiple linear regression, as we effectively filter out unwanted noise by retaining only the most strongly correlated PCs. The entire procedure is then reproduced for each data network and data layer to yield at least five ensemble reconstruction members for each season and sector. The number of ensembles for a given sea ice extent reconstruction is dependent on the number of additional data layers employed beyond the temperature and pressure observations.

Once all ensemble reconstructions are produced, the best-fit ensemble member (one for each season and sector of Antarctic sea ice extent) is first selected by extracting the reconstruction with the highest CE across all the ensemble reconstructions. To perform an additional check for model overfitting, the variance of the reconstruction in the period 1905–1978 is compared with the reconstruction variance in 1979–2020 and the observed variance in 1979–2020. If the reconstruction variance is significantly ($P < 0.01$) larger than the observed variance, there is a possibility of overfitting occurring. In these few cases, the best-fit reconstruction was selected as the next-highest CE where the variances were not statistically significantly different from the observed variance during 1979–2020, if possible. In some cases, there were no alternative reconstruction ensemble members with equal variances, and the highest CE was still selected as the best-fit reconstruction. This procedure was repeated for each season and sector to create the full array of ensemble and best-fit sector reconstructions.

The total reconstruction was produced separately following the above PC regression model, as was done for each sector. It was also estimated using the sum of the sector best-fit reconstructions, since the observed sea ice extent for all sectors sums to the total sea ice extent (purple lines in Fig. 2). Since each sector had multiple ensemble reconstructions, it is important to check how the sums of all possible ensemble member combinations across the sector compare. These combinations constitute more than 200,000 possible combinations for each season (there are over one million possible combinations in JJA). We therefore also provide an additional estimate from these combinations by selecting the combination that is most correlated with the observed sea ice extent time series (brown lines in Fig. 2). We use this and the full ensemble spread to further estimate reconstruction uncertainty. For others seeking to utilize these reconstructions in the future, we recommend using the full ensemble to best characterize the full uncertainty, and the best-fit reconstruction for all the sector reconstructions as the individual member with the highest skill. For total sea ice, the sum of the best-fit sector reconstructions is ideal to use for further study, as this is more reliable than the best-fit reconstruction calibrated to the total sea ice as described in the main paper.

As with many reconstructions, we assume that the physical relationships between southern hemisphere climate and Antarctic sea ice fundamental to our reconstruction procedure remain stationary throughout the twentieth century, which was previously verified for seasonal Antarctic pressure reconstructions[57]. We similarly assume that the boundaries for the Antarctic sea ice sectors remain fixed through time. These assumptions are partially tested by the verification statistics employed here as well as through the reconstruction ensemble. We are planning future work to fully address more of these assumptions in a coupled model framework.

Statistical methods. All correlations calculated in this work are the linear Pearson correlation coefficient. The statistical significance of correlation coefficients and regression coefficients (for linear trends of Antarctic sea ice extent) is calculated using a Student's t-test, with $n-2$ degrees of freedom. In making these calculations, we assume that each year is independent from every other year. To test for differences between the observations and reconstructed changes in two-year average seasonal sea ice extent, we compared the observed difference with the maximum magnitude of change we would see over the period of observation. This is to adjust for the selection of an extreme event to test. We computed the P value for a significance test compared with a null Gaussian distribution of differences using robust estimates of the location and scale.

Data availability

The reconstructions and the sea ice observations used to create them are all available on figshare[59] at https://doi.org/10.6084/m9.figshare.c.5709767.v1. Soon after publication, the sea ice extent reconstructions will also be made available through the NSIDC.

Code availability

The reconstruction and all figures were generated using the NCAR Command Language. All code used to generate the figures in this paper is available in the Antarctic Sea Ice collection on figshare at https://doi.org/10.6084/m9.figshare.c.5709767.v1.

References

44. *World Monthly Surface Station Climatology* (UCAR, 1981); https://rda.ucar.edu/datasets/ds570.0/
45. Zazulie, N., Rusticucci, M. & Solomon, S. Changes in climate at high southern latitudes: a unique daily record at Orcadas spanning 1903–2008. *J. Clim.* **23**, 189–196 (2010).
46. *Global Surface Summary of the Day* (National Centers for Environmental Information, 2021); https://www.ncei.noaa.gov/access/metadata/landing-page/bin/iso?id=gov.noaa.ncdc:C00516
47. Feistel, R., Hagen, E. & Grant, K. Climatic changes in the subtropical Southeast Atlantic: the St. Helena Island Climate Index (1893–1999). *Prog. Oceanogr.* **59**, 321–337 (2003).
48. Henley, B. J. et al. A tripole index for the Interdecadal Pacific Oscillation. *Clim. Dyn.* **45**, 3077–3090 (2015).
49. Huang, B. et al. Extended Reconstructed Sea Surface Temperature Version 4 (ERSST.v4). Part I: upgrades and intercomparisons. *J. Clim.* **28**, 911–930 (2015).
50. Mantua, N. J. & Hare, S. R. The Pacific decadal oscillation. *J. Oceanogr.* **58**, 35–44 (2002).
51. Enfield, D. B., Mestas-Nuñez, A. M. & Trimble, P. J. The Atlantic Multidecadal Oscillation and its relation to rainfall and river flows in the continental U.S. *Geophys. Res. Lett.* **28**, 2077–2080 (2001).
52. Fogt, R. L. & Marshall, G. J. The Southern Annular Mode: variability, trends, and climate impacts across the southern hemisphere. *WIREs Clim. Change* https://doi.org/10.1002/wcc.652 (2020).
53. Marshall, G. J. Trends in the southern annular mode from observations and reanalyses. *J. Clim.* **16**, 4134–4143 (2003).
54. Cavalieri, D. J., Gloersen, P. & Campbell, W. J. Determination of sea ice parameters with the NIMBUS 7 SMMR. *J. Geophys. Res. Atmos.* **89**, 5355–5369 (1984).
55. Comiso, J. C. Characteristics of Arctic winter sea ice from satellite multispectral microwave observations. *J. Geophys. Res.* **91**, 975 (1986).
56. Handcock, M. S. & Raphael, M. N. Modeling the annual cycle of daily Antarctic sea ice extent. *Cryosphere* **14**, 2159–2172 (2020).
57. Clark, L. & Fogt, R. Southern hemisphere pressure relationships during the 20th century—implications for climate reconstructions and model evaluation. *Geosciences* **9**, 413 (2019).
58. Cook, E. R., Meko, D. M., Stahle, D. W. & Cleaveland, M. K. Drought reconstructions for the continental United States. *J. Clim.* **12**, 1145–1162 (1999).
59. Fogt, R. Antarctic sea ice reconstructions. *Figshare* https://doi.org/10.6084/M9.FIGSHARE.C.5709767.V1 (2021).

Acknowledgements

All authors acknowledge support from the National Science Foundation Office of Polar Programs. R.L.F. and A.M.S. were supported by grant no. OPP-1744998, and M.N.R. and M.S.H. were supported by grant no. OPP-1745089.

Author contributions

R.L.F., M.N.R. and M.S.H conceived the study. R.L.F. and A.M.S. performed the reconstructions. R.L.F. led the writing of the manuscript and produced all the figures in the paper. All authors analysed the results and assisted in writing and editing the manuscript.

Competing interests

The authors declare no competing interests. Q7

Additional information

Extended data is available for this paper at https://doi.org/10.1038/s41558-021-01254-9.

Correspondence and requests for materials should be addressed to Ryan L. Fogt.

Peer review information *Nature Climate Change* thanks Sharon Stammerjohn, Elizabeth Thomas and the other, anonymous, reviewer(s) for their contribution to the peer review of this work.

Reprints and permissions information is available at www.nature.com/reprints.

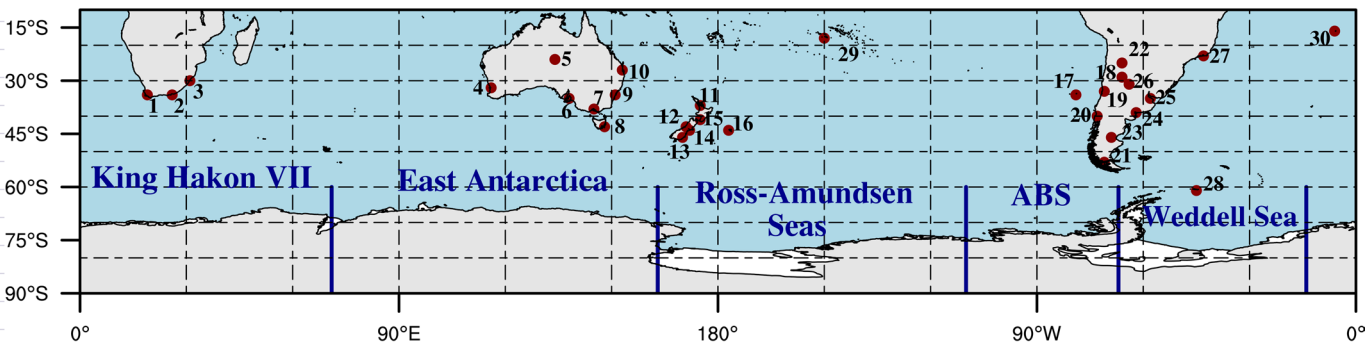

Station Names

1. Cape Town
2. Port Elizabeth
3. Durban
4. Perth
5. Alice Springs
6. Adelaide
7. Melbourne
8. Hobart
9. Sydney
10. Brisbane
11. Auckland
12. Hokitika
13. Dunedin
14. Christchurch
15. Wellington
16. Chatham Island
17. Juan Fernandez
18. Catamarca
19. Santiago
20. Valdivia
21. Punta Arenas
22. Salta
23. Sarmiento
24. Bahia Blanca
25. Buenos Aires
26. Cordoba
27. Rio de Janeiro
28. Orcadas
29. Tahiti
30. St. Helena Island

Additional Climate Index Data Layers

Interdecadal Pacific Oscillation (IPO)
Atlantic Multidecadal Oscillation (AMO)
Pacific Decadal Oscillation (PDO)
Southern Oscillation Index (SOI)
Nino 1+2 SST Anonamlies
Nino 3.4 SST Anomalies
Nino 3 SST Anomalies
Nino 4 SST Anomalies
Southern Annular Mode Seasonal Reconstructions

Extended Data Fig. 1 | Map of predictor stations, additional climate index data layers, and sea ice sectors. Sea ice sectors are defined as in Raphael and Hobbs (2014). Station data are primarily from the University Corporation for Atmospheric Research research data archive dataset ds570.0 (https://rda.ucar.edu/datasets/ds570.0/#!description). See Methods for a more detailed description of data sources and sea ice sectors.

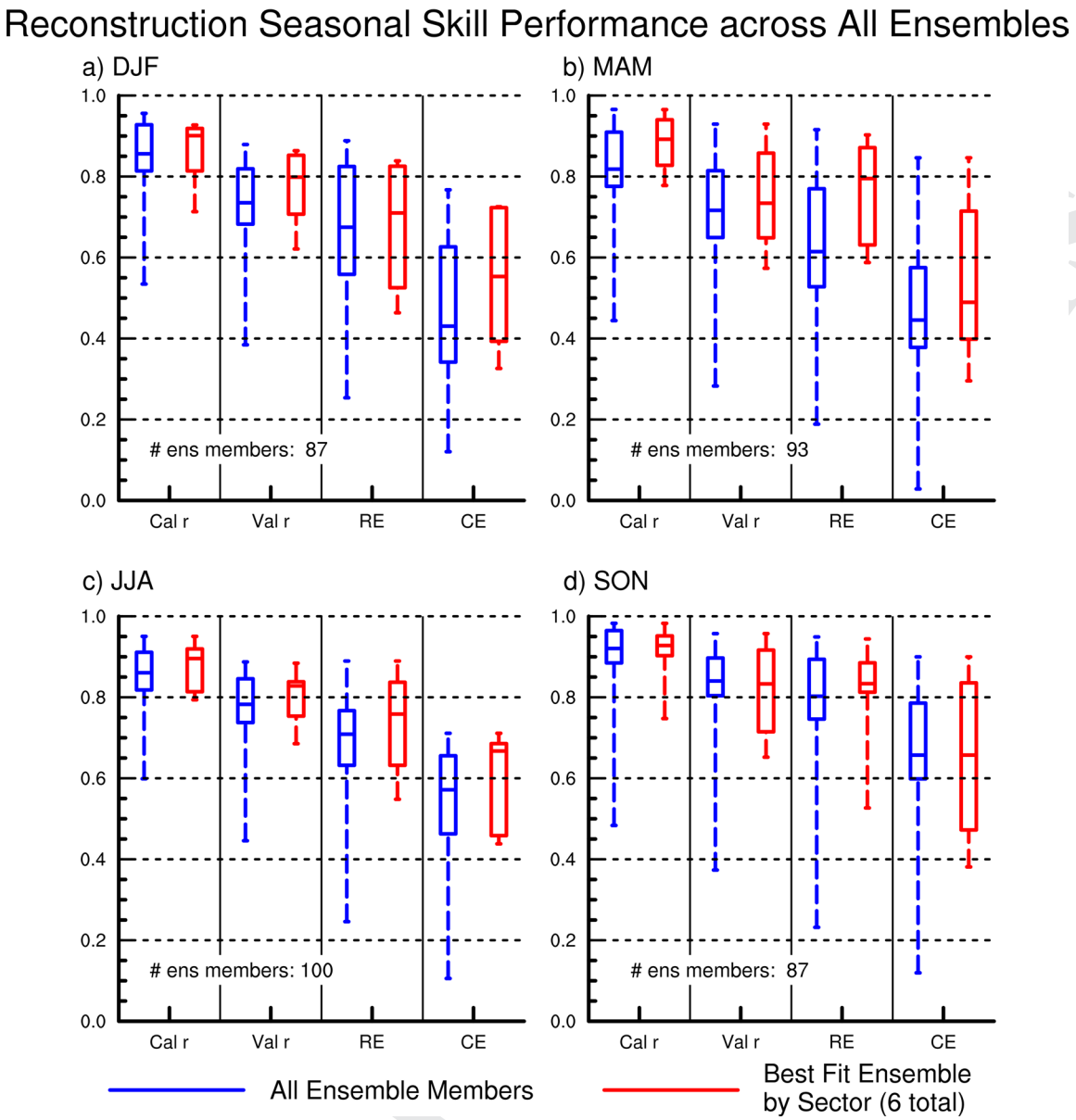

Extended Data Fig. 2 | Boxplots of reconstruction performance. Boxplots for reconstruction performance across all ensembles are in blue, and the best fit reconstruction for each sector, including total are in red. The vertical lines extend to the minimum and maximum for each skill metric, and the boxes extend to the upper and lower quartiles. The median for each distribution is given with the horizontal line in the middle of each boxplot.

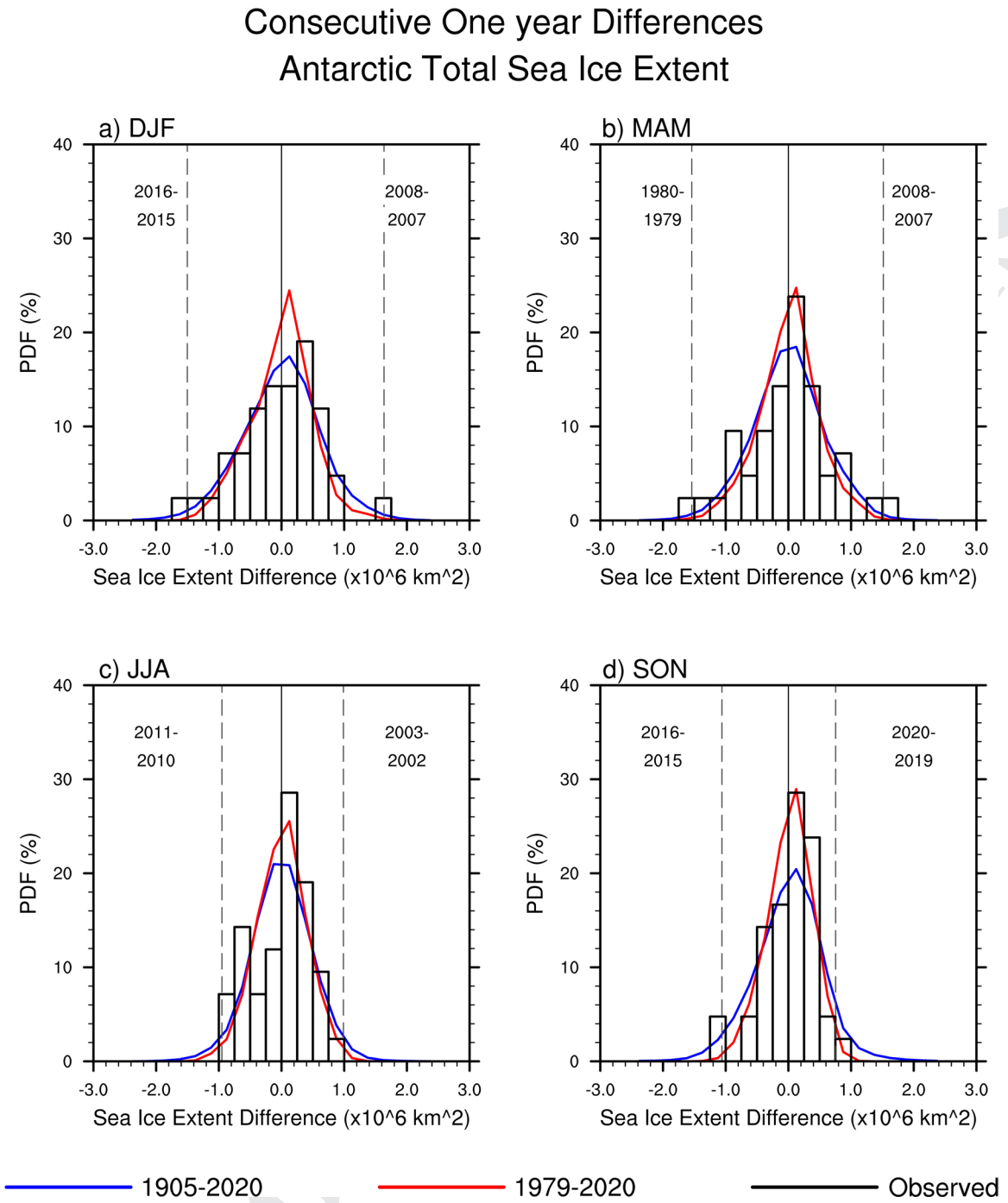

Extended Data Fig. 3 | Changes in year-to-year seasonal sea ice extent. Seasonal probability distribution functions (PDF, in %) for differences (following year minus preceding year) in consecutive one year values in observed Antarctic total sea ice extent (black, plotted as a bar chart) and in all Antarctic total sea ice extent ensemble members from 1979–2020 (red) and 1905–2020 (blue). The dashed vertical lines indicate the minimum and maximum differences in observations, with the years corresponding to these record differences given in the upper corners within each panel.